Repro Copy:

N72-28802

FINAL REPORT
ANALYSIS OF INNER AND OUTER ZONE OGO-1 AND OGO-3 ELECTRON SPECTROMETER AND ION CHAMBER DATA

MAY 1972

MDC G2960

PREPARED BY

DR. K. A. PFITZER
PRINCIPAL INVESTIGATOR
SPACE SCIENCES DEPARTMENT

CONTRACT NASW-2203

MCDONNELL DOUGLAS ASTRONAUTICS COMPANY-WEST

5301 Bolsa Avenue, Huntington Beach, CA 92647

CONTENTS

I. INTRODUCTION

The OGO-1 and OGO-3 satellites provided data for a number of interesting investigations because of their sophisticated instrumentation, long life, and very elliptical and slowly precessing orbits. This study extends some of the earlier work using the University of Minnesota electron spectrometer and ion chamber data from OGO-1 and 3. The electron spectrometer on OGO-1 and 3 was the first instrument to successfully measure the electron spectrum in the inner zone without bremsstrahlung and proton contamination. Preliminary studies have indicated that radial diffusion theory may be used to predict the time history of the inner zone. This study uses the available inner zone data from OGO-1 and 3 to calculate the best fit diffusion coefficient for the inner zone.

By correlating the OGO data with data from the ATS-1 satellite, drift shell splitting was experimentally verified and substorm drift effects were first observed (Pfitzer and Winckler, 1969; Pfitzer et al., 1969). By further extending the correlation to include plasma data from Pioneer 7 and Explorer 33, it will be shown that a time dependent magnetic field model more accurately predicts the behavior of charged particles in the magnetic field. The study takes into account solar wind induced variations in the magnetospheric magnetic field by changing the Mead-Williams (1965) input parameter R_S, the stand off distance, from a constant to a solar wind pressure dependent parameter.

A third unique study made possible by the varying orbits of OGO-1 and 3 is the study of the high energy trapping boundary. A number of satellites have studied the boundary at either the equator or in the high latitude low altitude region. The OGO-1 and 3 satellites, which were initial placed into nearly equatorial orbits, slowly precessed to nearly polar orbits. Thus the complete high energy trapping boundary was sampled during the lifetime of the satellites.

This study continues the investigation of dynamic processes which govern the acceleration and loss of electrons in the radiation zones and tests the applicability of diffusion theories to describe the motion of the electrons within the radiation belts. The study also tests the accuracy of several magnetic field models by comparing predicted drift shell geometries with observed electron drift shells.

II. INNER ZONE DIFFUSION

A. Review

The process of diffusion in the magnetosphere plays an important role in the study of electron acceleration. Examples of diffusion-like behavior have been known for some time (Frank, 1965a). A study of the diffusion process is complicated by the fact that several processes are generally operating simultaneously and the diffusion process may not be identifiable. On several occasions the distribution of electrons was altered in a manner which allowed the diffusion process to be separated and the diffusion coefficient isolated. An example is the nuclear explosion of November 1, 1962 from which unambiguous determination of the diffusion coefficients were made (Newkirk and Walt, 1968). The geomagnetic storms of April 1965, August 1966, and May 1967 present a unique opportunity to study the diffusion process over an extended region in the inner zone. This study will determine the radial diffusion coefficient from L = 1.6 to L = 2.2 for electrons in the energy range 50 keV to 4 MeV.

B. The Diffusion Equation

The time dependent diffusion process which conserves the first two adiabatic invariants μ and J is given by (Newkirk and Walt, 1968)

$$\frac{\partial n}{\partial t} = \frac{\partial}{\partial L}\left(\frac{D}{L^2}\frac{\partial}{\partial L}\, nL^2\right) - \frac{n}{\tau(L)} \tag{1}$$

where $n(\mu, J, L, t)\, d\mu dJ dL$ is the number of electrons in an element $d\mu dJ dL$, μ and J being the first and second invariants, $\tau(L)$ is the pitch angle loss rate and L being the McIlwain parameter. For equatorial electrons (i.e., electrons having an equatorial pitch angle of 90 degrees) J = 0.

The first adiabatic invariant has the form

$$\mu = p^2/2m_oB$$

$$= \frac{1}{2B} \frac{E_k\left(E_k + 2m_oC^2\right)}{m_oC^2}$$

$$= \frac{E_k}{2B}(\gamma + 1) \tag{2}$$

where p is the electron's momentum, E_k its kinetic energy, γ the relativistic constant, and B the magnetic field at the position of the electrons. B is assumed to have the value $0.31/L^3$. The distribution function n can be shown to have the form

$$n \propto \frac{Lj_\perp}{\mu} \tag{3}$$

where $j_\perp = dJ/dE$, the differential energy flux having an equatorial pitch angle of 90 degrees. Since the analysis is performed at constant μ, $n \propto Lj_\perp$ and hence

$$L^2n \propto L^3j_\perp \tag{4}$$

The radial diffusion coefficient D is assumed to have the value $D = AL^m$ such that

$$\frac{\partial n}{\partial t} = \frac{\partial}{\partial L}\left[AL^{m-2}\frac{\partial}{\partial L}L^2n\right] - \frac{n}{\tau(L)} \tag{5}$$

The above differential equation was computer integrated to give a best fit in space and time to the data.

C. Presentation of Data

The available data consist of electron spectrometer measurements from the OGO-1 and OGO-3 spacecraft in 5 energy channels from 50 keV to 4 MeV (50-120 keV, 120-290 keV, 290-690 keV, 690-1700 keV, and 1700-4000 keV). The experiment is described in detail in previous publications (Pfitzer, 1968). The data are available in the form of $j(\alpha_o, E, t, L)$, the differential flux as a function of the equatorial pitch angle, energy, time and L.

It has been shown by Pfitzer (1968) that in the inner zone the flux changes very slowly and that the shape of the pitch angle distribution remains constant during the entire 3 year history of the OGO-1 and OGO-3 electron data. This indicates that we may write

$$j(\alpha_o, E, t, L) = j(\alpha_o, E, L)\,\epsilon(t) \tag{6}$$

It has also been shown that the equatorial pitch angle distribution can be approximated very accurately by the function

$$g(\alpha_o) = 10^{\beta} \tag{7}$$

where

$$\beta = \sum_{j=1}^{N} A_j (90 - \alpha_o)^{2j} \tag{8}$$

and where the Aj are determined by least squares best fits. Therefore for a given energy and L

$$j(\alpha_o, t) = g(\alpha_o) \cdot \epsilon(t) \tag{9}$$

and hence the pitch angle dependence of the data can be removed by the equation

$$j(t) = j(90, t) = \frac{g(90)}{g(\alpha_o)}\, j(\alpha_o, t) \tag{10}$$

In this way all of the data are normalized to α_o = 90 degrees. Figure 1 shows the equatorial fluxes at L = 2.2 before the onset of the April 1965 solar cosmic ray event and one month after the event. No detectable change in the shape of the pitch angle distribution is observed at L = 2.2 or at any other L in the inner zone due to the storm. Therefore the data during the decay phases of the storm may also be normalized to α_o = 90 degrees giving rise to the dJ/dE versus time curves shown in Figure 2.

Figure 2 gives an example of the pitch angle normalized data (for 290-690 keV electrons during the September and May events). After the September event, for L = 1.5, the rate increased slowly over a period of 30 or more days. When a new level was reached no rapid decay was evident and the new level was stable. At L = 2.0 the increase was more rapid reaching a peak less than 5 days after the event began. This level was maintained for 30 days and then an exponential decay dropped the count rates to a new and apparently stable level. For L ≥ 2.2 the increases were large and the exponential decay immediately returned the rates to prestorm levels

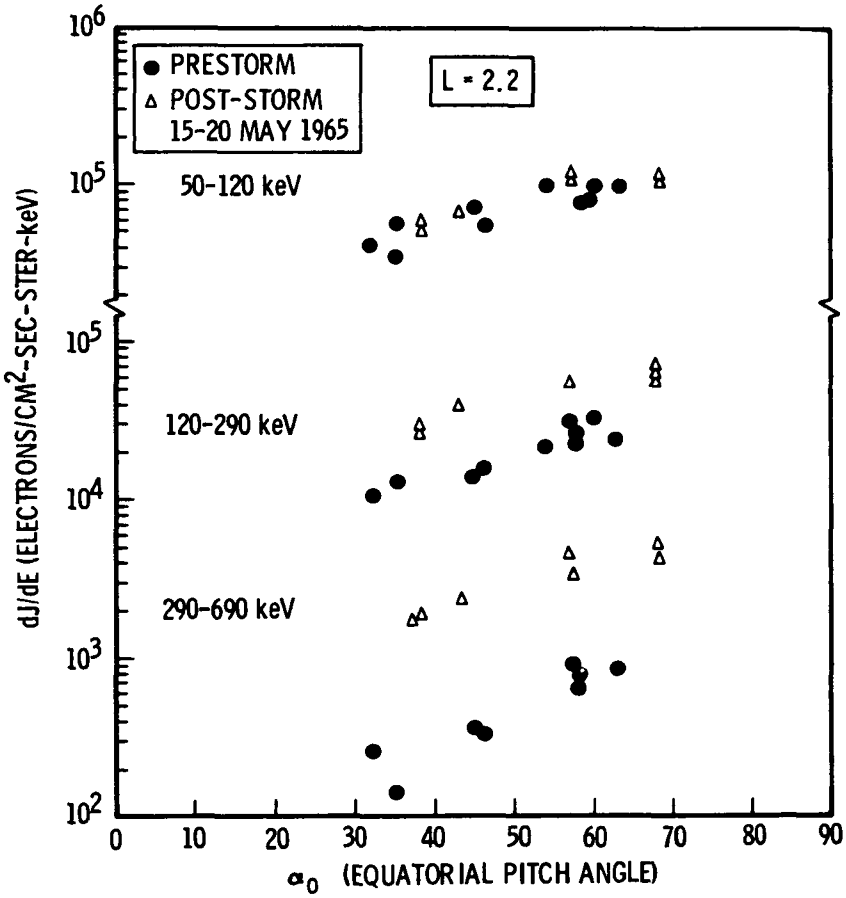

Figure 1. Pre-storm and Post-storm Equatorial Pitch Angle Distribution

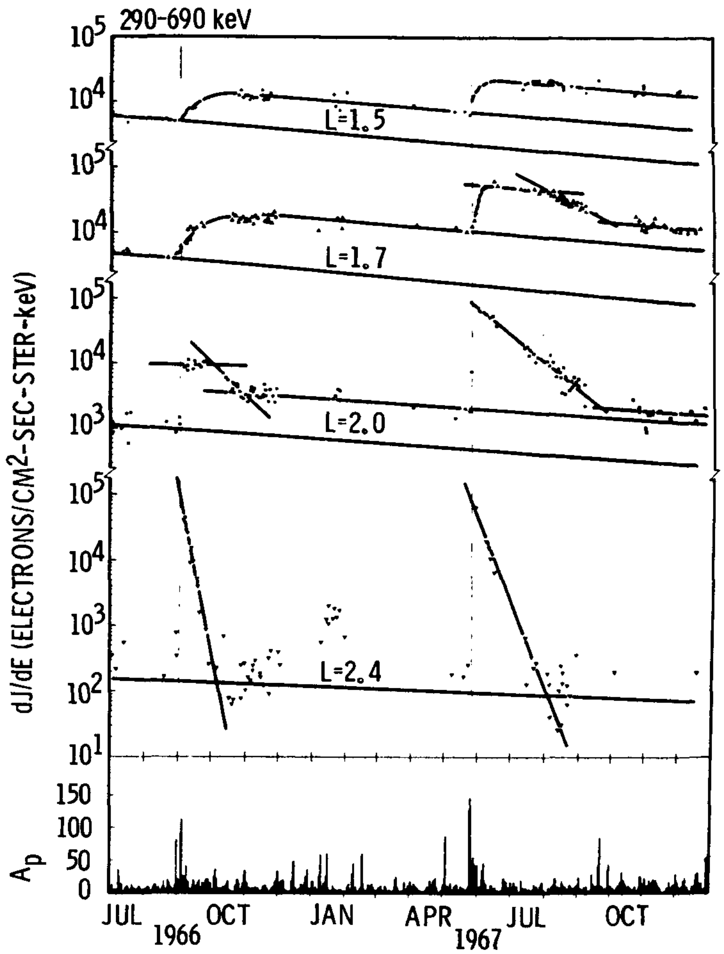

Figure 2. Flux Versus Time Profiles

within 30-40 days after the onset of the event. The above discussed behavior is very indicative of a sudden impulsive increase during the main phase of the storm followed by a period of diffusive rearrangement lasting several months. It is this rearrangement which offers a unique opportunity to solve the diffusion equation.

In order to solve the diffusion equation, the data must be converted from fluxes at constant energy to a distribution function at constant μ. Since we will only deal with the pitch angle normalized equatorial data, $\mu = p/2m_oB$. B was assumed to have the form $B = 0.31/L$ for equatorial trajectories. Beginning with the pitch angle normalized data points at a given L and t, flux versus energy plots were obtained for the periods April 5 through June 15, 1965; August 15 through December 1, 1966; and May 15 through December 1, 1967 (see Figure 3 for an example). Best fit curves were then

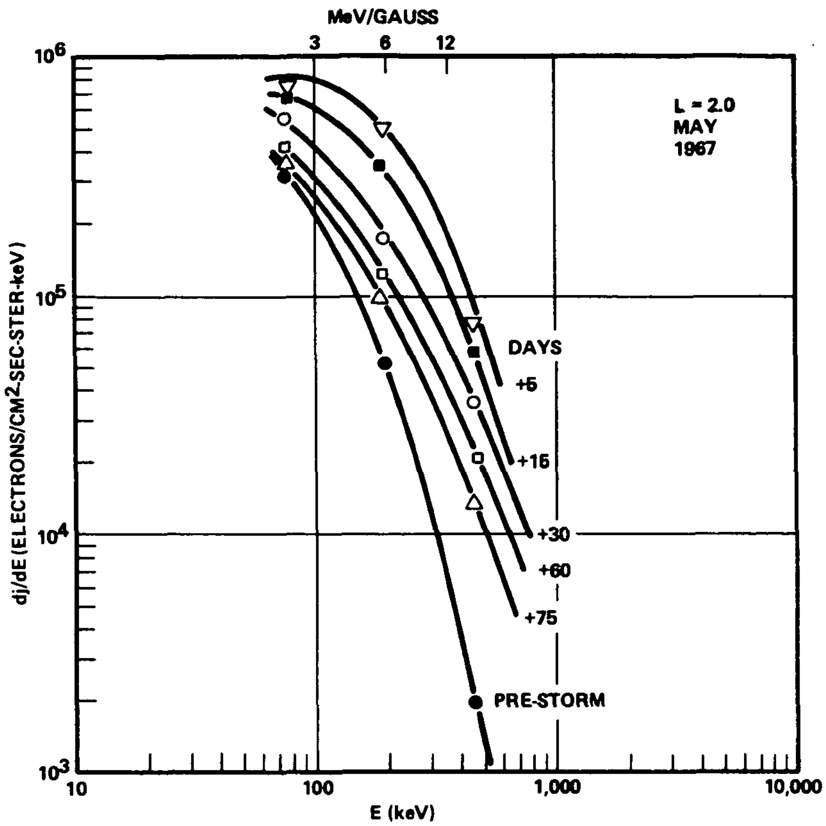

Figure 3. Differential Energy Spectra

drawn through these data points giving the differential energy spectra versus energy at a given time and L. Subsequently a μ axis is attached to each of these figures where

$$\mu = p^2/2m_oB = E_k \ (\gamma+1) \ L^3/0.62 \ \cdot \qquad (11)$$

These best fit differential energy spectra curves versus μ then become the working data set from which all subsequent data for the diffusion analysis are obtained.

Using the differential energy spectra, plots of the differential energy flux at fixed t, μ and at $J = 0$ are plotted versus L (see Figure 4 and 5). The distribution function is obtained from this curve by using the fact that n is proportional to the differential flux multiplied by L/μ. A further manipulation converts the data to a plot of L^2n versus L (see Figure 6). The log of

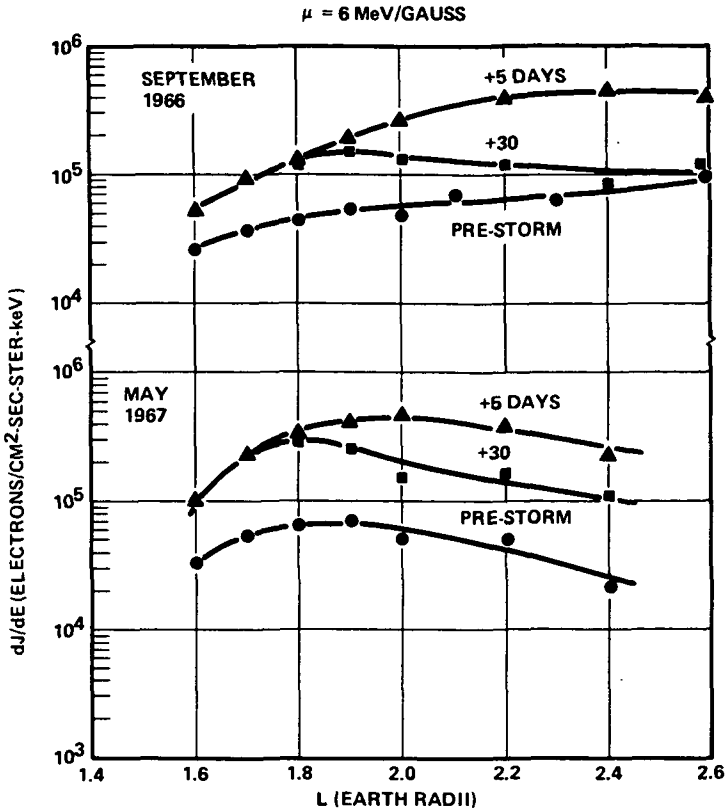

Figure 4. Differential Energy Flux

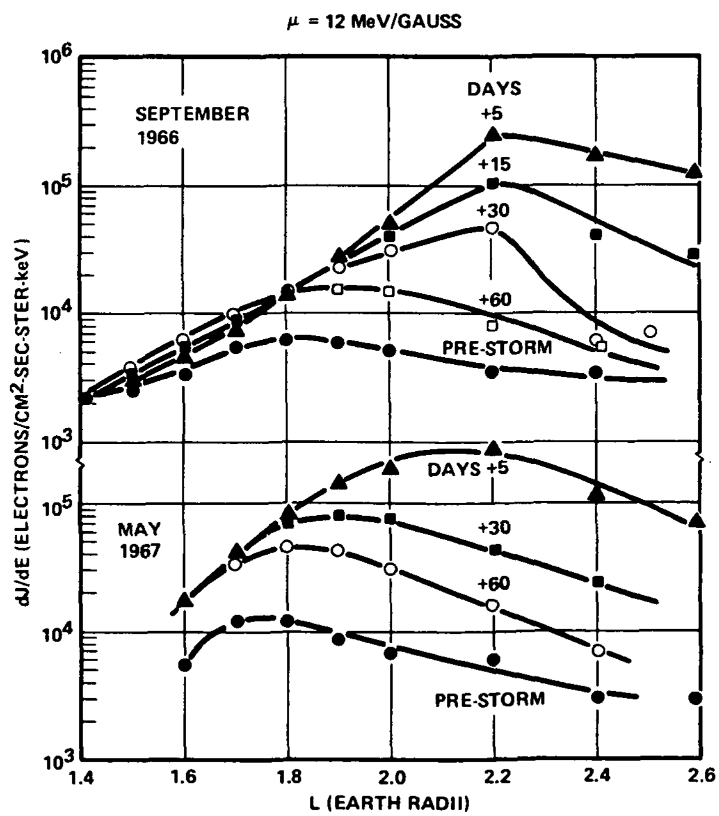

Figure 5. Differential Energy Flux

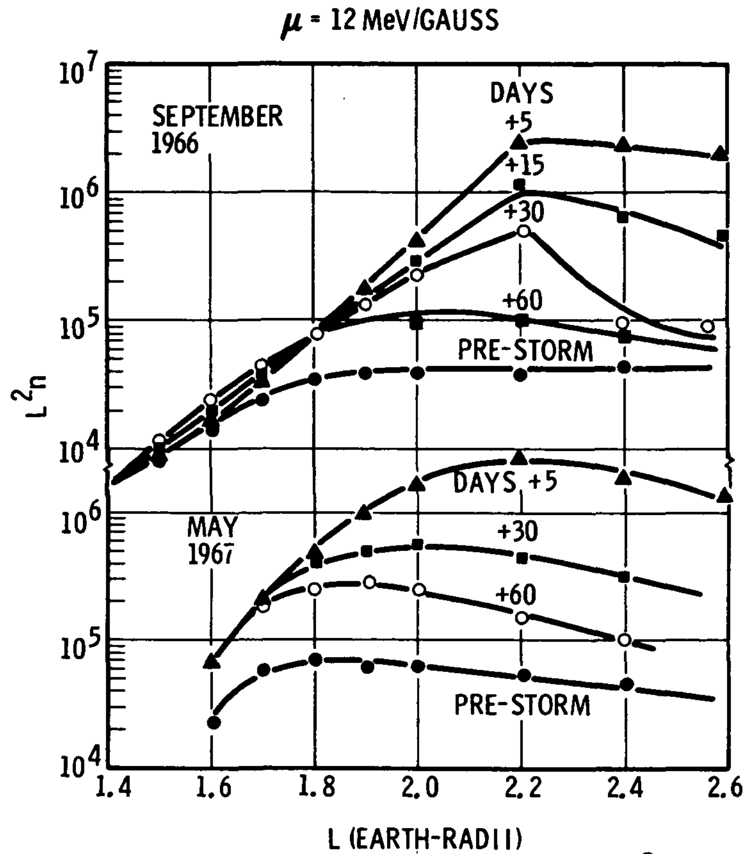

Figure 6. Distribution Function Multiplied by L^2

the data points in Figure 6 is fitted with a least square polynomial fit in preparation for computer integration of the equation. The boundary conditions imposed during this integration are such that n is held constant at L = 1.3 and at L = 4.0. The available data verify this boundary condition as a reasonable approximation.

The data at μ = 6 MeV/gauss have relatively few distinct features and only limited changes in the radial gradients (see Figure 4). When μ = 6Mev/gauss our analysis was unable to explicitly separate D, the radial diffusion term and τ, the pitch angle diffusion term. However, Figure 6, which shows the data at μ = 12 MeV/gauss, has very distinct and radically different radial gradients as a function of time. Radial diffusion and pitch angle diffusion was, therefore, separated for 12 MeV/gauss.

D. Conclusion

A best fit analysis of the diffusion equation using the OGO-1 and OGO-3 data gives a value of $1.0 \times 10^{-6} L^{10}$ for D, the diffusion coefficient when μ = 12 MeV/gauss (580 keV electrons at L = 1.6). The analysis is valid in the region $1.6 \leq L \leq 2.2$. The μ dependence of the diffusion coefficient could not be determined from this analysis.

The above determination of the diffusion coefficient for electrons (see Figure 7) is in an energy range and L range where there currently exist only limited data. The result agrees quite well at the lower L value with the work of Farley (1969). Farley's determination of the diffusion coefficient was based on the decay of the Starfish electrons and is in an energy range (363 keV at L = 1.55) close to the energy range of this calculation. The current result, however, is much larger than the results of Walt (1971) and Newkirk and Walt (1968) whose determination uses the diffusive spreading of the ARGUS and USSR nuclear explosions and are at an energy considerably higher than that of the current analysis.

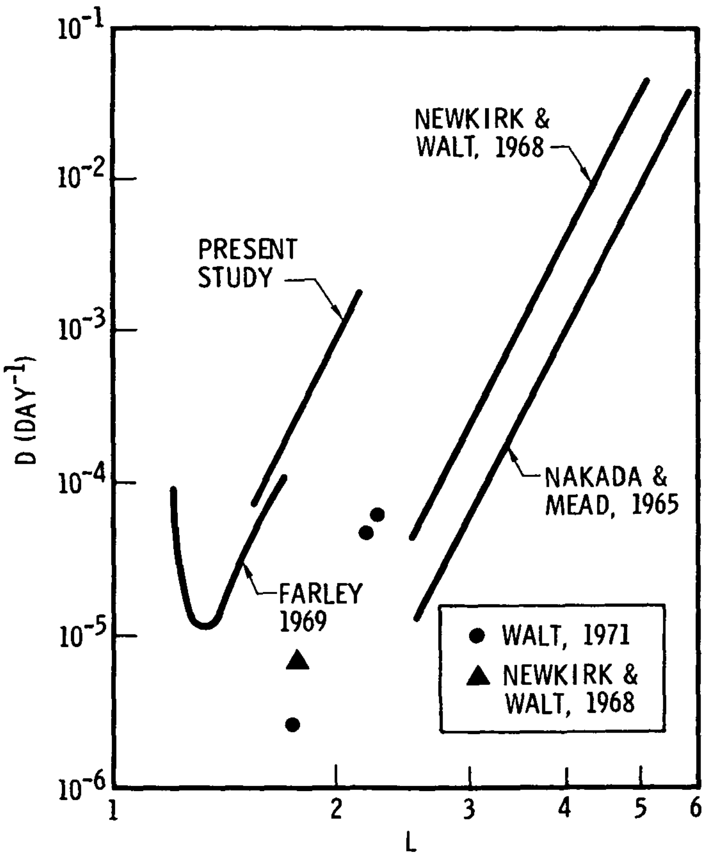

Figure 7. Radial Diffusion Coefficients for Electrons

"Page missing from available version"

III. DRIFT SHELL SPLITTING ASYMMETRIES

A. Review

Data from an electron spectrometer on the synchronous orbit satellite, ATS-1, (Lezniak et al., 1968; Lezniak and Winckler, 1968) and data from the electron spectrometer and ion chamber on the elliptic orbit satellite, OGO-3, (Kane, 1967; Pfitzer, 1968; Pfitzer and Winckler, 1968) can be used to test experimentally the drift shell splitting of trapped electrons in the distorted dipolar field of the magnetosphere. Northrop and Teller (1960) pointed out that in cases where the magnetic field lacks axial symmetry, gradients of B occur in the azimuthal direction which produce radial drift motions of trapped particles and that this radial drift will vary with the equatorial pitch angle of particles found at a given point in the magnetic field. Thus, even with the conservation of the first and second adiabatic invariants of motion, particles which after drifting around the earth return to their point of origin nevertheless at intermediate points will be found on different drift shells depending on pitch angle. This is in contrast to a magnetosphere described by a pure dipole field, where all particles which initially start at the same point remain on the same drift shell independent of pitch angle or energy. Near the earth ($r < 5\ R_e$) the distortion of the earth's field is small and the drift shells of particles having different pitch angles are almost identical, a fact contained in the McIlwain L-parameter approximation which is useful for mapping particle fluxes at such low L values. However, in the vicinity of the ATS-1 orbit ($6.6\ R_e$) the distortion of the magnetic field can be quite large due to currents on the magnetosphere boundary and currents in the tail. Theoretical studies of the motion of trapped particles in the distorted dipolar field have been carried out by Hones (1963), Fairfield (1964) and Mead (1966). This work has been extended by Roederer (1967) who has used the Mead model magnetic field (Mead, 1964; Williams and Mead, 1965; Mead, 1966) which has given reasonably good quantitative agreement with experimental measurements of the magnetic field. Pfitzer et al. (1969)

experimentally verified the concept of drift shell splitting by using ATS-1 magnetometer data, ATS-1 electron spectrometer data and OGO-3 electron spectrometer data. Using the Mead model magnetic field for calculating the drift shells for electrons having pitch angles of α_0 = 65 degrees and α_0 = 90 degrees, as well as the measured pitch angle distributions and measured radial gradients for electrons at local noon, the pitch angle distribution was calculated as a function of local time for the ATS-1 orbit. The agreement between calculated and measured pitch angle distribution is satisfactory not only in predicting the proper noon to midnight asymmetry (25 to 1 for 500-1000 keV electrons on February 15, 1967) but also in correctly predicting the pitch angle distribution as a function of local time (isotropic at noon but non-isotropic with a 3 to 1 ratio between α_0 = 65 degrees and α_0 = 90 degrees at midnight). However, in one case (February 15, 1967) an asymmetry is observed about local midnight with minimum count rate at 2200 LT, representing a departure from the symmetric Mead model (see Figure 8).

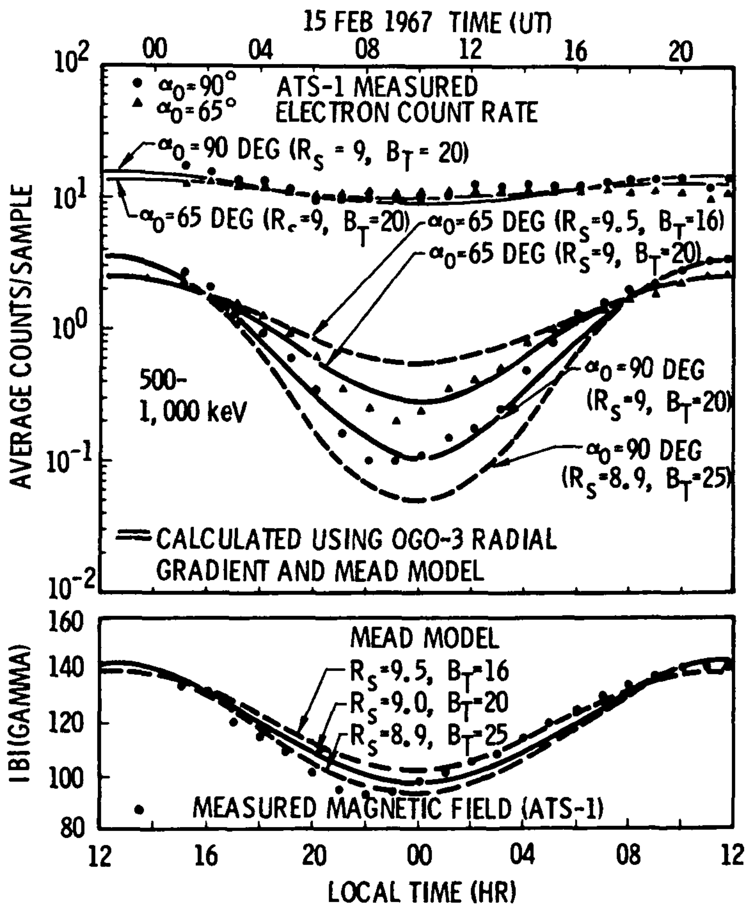

Figure 8. Local Time Profiles

It was suggested that these asymmetries were too large to be accounted for by using the tilted dipole model and, therefore, the asymmetries were most likely caused by either the asymmetric ring current or by convective flow within the magnetosphere (Pfitzer et al., 1969). However in this study we show that observations of the solar wind pressure during this time period indicate that changes in the solar wind number density and velocity can easily account for the observed asymmetry. The study relating changes in the solar wind pressure to the observed asymmetry is presented below.

B. Presentation of Data

Roederer (1969) has shown that by varying the input parameters to the Mead-Williams model (i.e. the stand-off distance, R_S, and tail field strength, B_T) as a function of time, the magnetic field values predicted by the model may be adjusted to accurately represent the time history of the magnetic field as observed by ATS-1. Furthermore, Roederer showed that this method of determining the stand-off distance was valid by a comparison of his results with Vela boundary crossing measurements. The stand-off distance R_S may also be calculated from the equation

$$R_S = (M^2/4\pi\ nmv^2)^{1/6} \quad \text{(Mead, 1964)} \qquad (12)$$

where M is the earth's magnetic moment, n is the particle number density, m is the mass of a particle, and v is the bulk speed. Plasma data measurements from Pioneer 7 (H. S. Bridge, MIT) and Explorer 33 (H. S. Bridge, MIT) which were obtained from the National Data Center were substituted into the above equation for several time periods during January, 1967. The stand-off distance thus calculated is then compared to Roederer's measurements (Figure 9). There is excellent agreement between the stand-off distance as calculated from ATS-1 magnetometer data and the stand-off distance calculated from solar wind parameters.

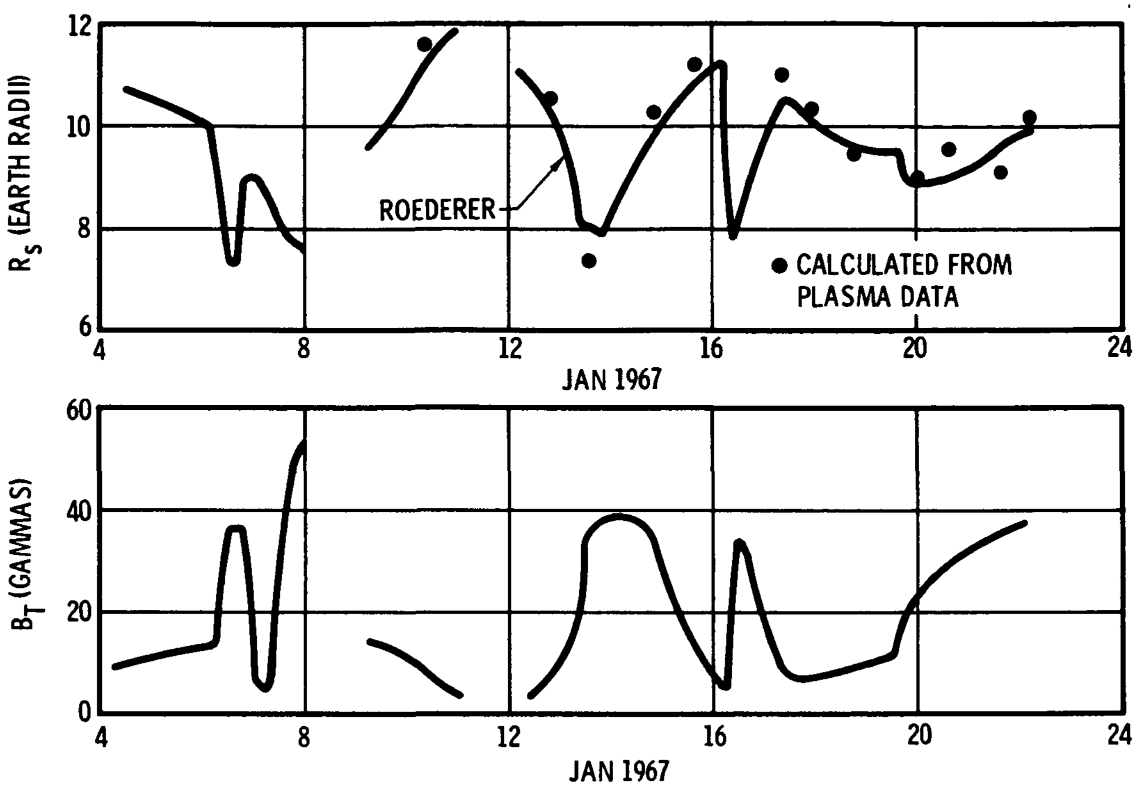

Figure 9. Comparison of Plasma Determined Standoff Distance with That Obtained by Roederer

Since we have shown that the behavior of the stand-off distance over a period of 1 month may be calculated from plasma measurements, we now apply the correlation between the plasma data and stand-off distance to short term fluctuations (< 1 day). By inputing the stand-off distance time variations as calculated from the plasma data, we expect to model changes in the magnetic field caused by changes in the stand-off distance. The density and bulk speed as measured by Pioneer 7 and Explorer 33 are plotted in Figure 10. The density and speed are input into the stand-off distance equation and the calculated values of R_S are then plotted inFigure 11 along with the tail field parameter B_T. B_T is assumed to have the general inverse correlation to R_S determined by Roederer.

Using R_S and B_T as a function of time we now use the drift shell program of J. Roederer which uses McIlwain's field line program to calculate the drift shells passing through ATS-1 at $r = 6.6\ R_e$ and various local times for electrons having pitch angles of $\alpha_o = 90$ degrees and $\alpha_o = 65$ degrees. Applying the calculation techniques described by Pfitzer et al. (1969) which use

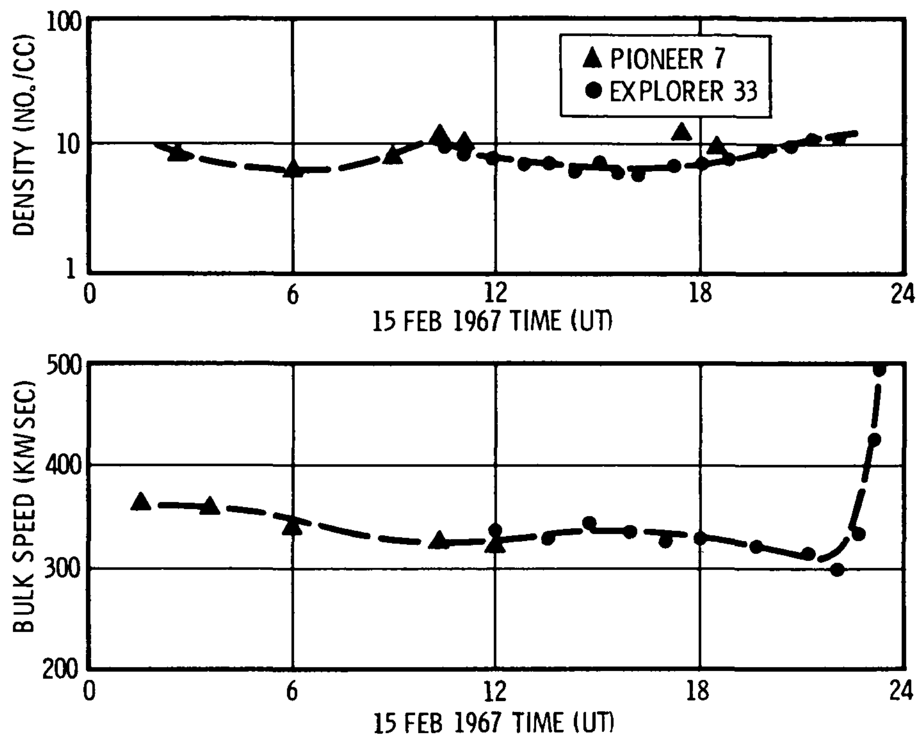

Figure 10. Measured Plasma Density and Speed

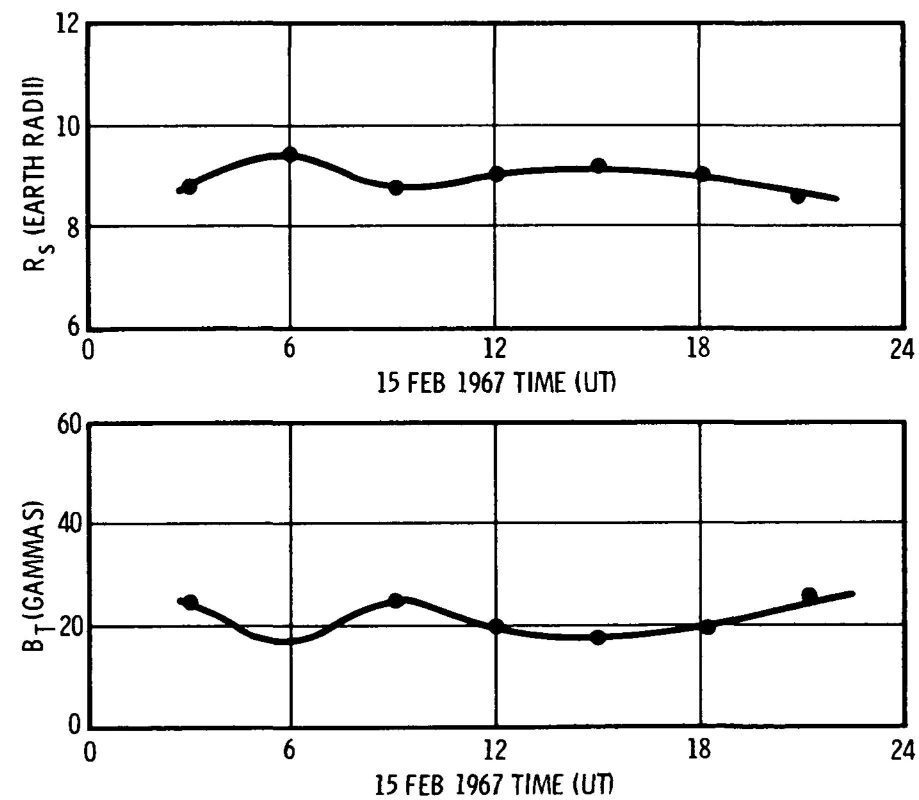

Figure 11. R_s and B_T as Determined from Plasma Pressure

the electron pitch angle distributions measured by ATS-1 at local noon and the radial gradient measured by OGO-3 at local noon, we calculated the local time dependence for the magnetic field for electrons having pitch angles of α_o = 65 degrees and α_o = 90 degrees at midnight). However, in one case There is excellent agreement between the calculated and observed local time dependence. The result obtained using a time dependent R_S and B_T correctly predicts the observed 30 degree asymmetry.

C. Discussion

Using a time dependent R_S and B_T, where R_S is calculated as a function of time from the stand-off distance equation, as the input parameter into the Mead-Williams field model significantly improves the agreement between theory and data. The observed asymmetry on Feb. 15, 1967 can be explained by changes in the solar wind plasma pressure causing changes in the stand-off distance which cause changes in the magnetic field. We must, therefore, conclude that the asymmetric ring current and other convective flows within the magnetosphere were not important on Feb. 15, 1967, since

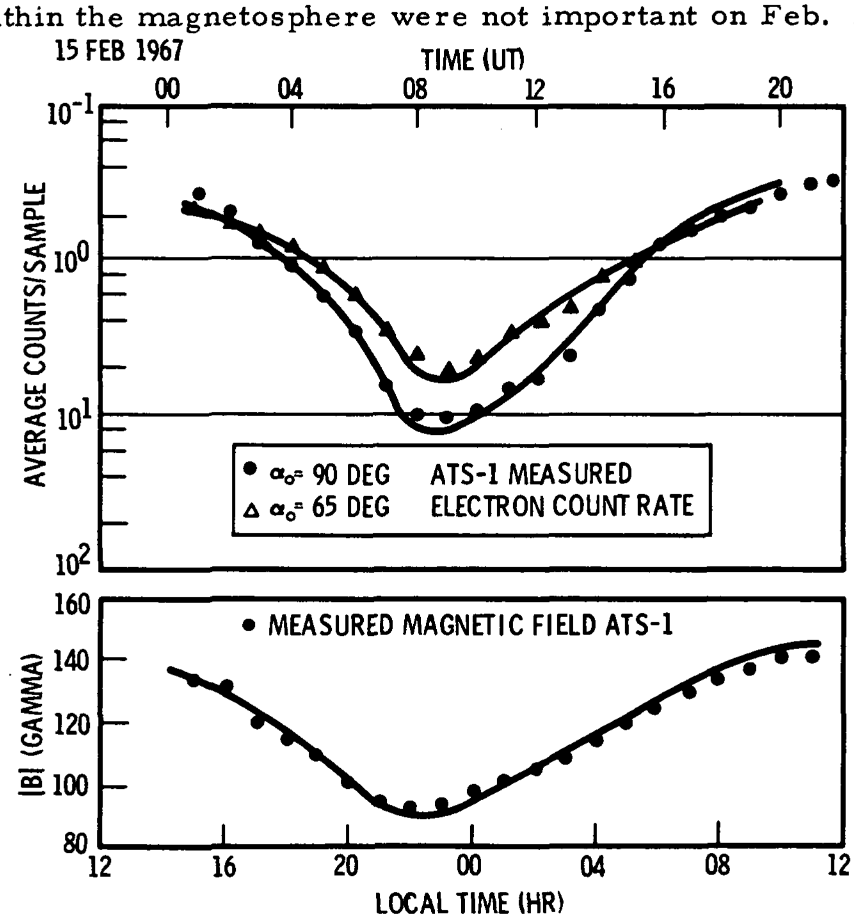

Figure 12. Comparison of Data with Plasma Pressure Corrected Models

the solar wind fluctuation produced effects comparable to those observed. We have shown that prior to discussing observed local time asymmetries in the magnetic field strength and particle flux, we must take into account changes which can be attributed to changes in the solar wind. Having removed these external effects it may then be possible to study locally produced asymmetries and quantitatively study the energization and distribution of the trapped electrons. It has also been shown that the stand-off distance as calculated from the plasma data can be used as a time dependent input to the magnetic field models to more accurately predict the magnetic field within the magnetosphere.

"Page missing from available version"

IV. HIGH ENERGY TRAPPING BOUNDARY

A. Introduction

Observations of energetic electrons inside the magnetosphere and in the transition region (Frank, 1965b) show that a relatively stable core of medium energy electrons ($E \geq 40$ KeV) of intensity $10^7 - 10^8$ electrons/cm^2 sec surrounds the earth. This core of electrons extends to the magnetopause (~10 earth radii) in the solar direction and to a distance of about 8 earth radii in the anti-solar direction. Close to the geomagnetic equatorial plane and within about 45 degree longitude of the sub-solar point, the intensity of these medium energy electrons is found to terminate coincidently with the magnetopause.

The spacial distribution of energetic electrons ($E > 1.6$ MeV) is generally believed to lie within this relatively stable core of medium energy electrons. Large intensity spikes of both medium energy and energetic electrons have been observed mostly outside this stable core of electrons. It is of interest to determine the region of space in which the stable core of electrons is confined.

A detector outside the stable core of electrons would, except for occasional spikes of intensity, count only the background due to cosmic rays. The OGO-1 and OGO-3 ion chambers were designed to make precise measurements of cosmic ray ionization; whereas, OGO electron spectrometers were designed to measure trapped electrons. They are, therefore, well suited to determine, to a considerable precision, the boundary of the stable core of energetic electrons. Since the ion chamber has a several orders of magnitude lower sensitivity threshold than the electron spectrometer and since the ion chamber by virtue of its intercalibration with the spectrometer is known to count only electrons in this region of space, it is used for the boundary determination.

The OGO-1 and 3 spacecraft are particularly useful for this study. Although they were initially placed into highly elliptical nearly equatorial orbits (orbital inclination of ~30 degrees to the geographic equator), the interaction of the satellite with the moon precessed these orbit out of the equatorial planes to higher latitudes. After two years the OGO-1 and 3 orbital inclination changed from 30 to 50 degrees. This presented the unique opportunity to study the trapping boundary from the equatorial plane to the polar high latitude cut-offs with the same instrument giving rise to the opportunity to study the shape of the field lines along which the last permanently trapped electrons are to befound. A comparison between the measured boundary and the boundary calculated using several available magnetospheric models points out some of the shortcomings of these models. The comparison of the data with the models require a considerable precision of the models since we not only check the models at individual points but require that the model be accurate over a large region in order to correctly predict field line and drift shell geometries. Small errors in the models when integrated over large regions of space give rise to easily measurable discrepancies.

B. Response Characteristics of the Ion Chamber

Since the determination of the boundary of the energetic electrons depends on the sensitivity of the detector to these particles, it is necessary to discuss the characteristics of the detector in some detail. The operation of the ion chamber and determination of the response characteristics are described elsewhere (Kane et al., 1966). A summary of the main characteristics is presented in Table I. The ion chamber responds directly to protons above about 12 MeV and to electrons above about 0.7 MeV. The ion chamber also responds to lower energy electrons through the bremsstrahlung they produce in the chamber wall. The response characteristics for the penetrating and non-penetrating electrons are shown in Figure 13. It can be seen that, as far as electrons are concerned, the chamber responds predominantly to electrons with energy ≥ 0.7 MeV. In the region of interest (outer radiation zone and beyond) the electrons above 0.7 MeV are believed to be much larger in number than protons of energy >12 MeV. In these regions, therefore, the OGO-1 and 3 ion chambers can be considered as omnidirectional detectors

Table I

OGO-1 ION CHAMBER

Omnidirectional Projected Area	250 cm^2
Argon Pressure	50 lb. /in. ^{2}
Minimum Energy Penetration	
Protons	12 MeV
Electrons	0.7 MeV
Average Ionization due to 1 electron/cm^2 sec	
40 keV	8.3×10^{-7} norm. pulses/sec x 10^3
0.7 MeV	5.5 norm. pulses/sec x 10^3

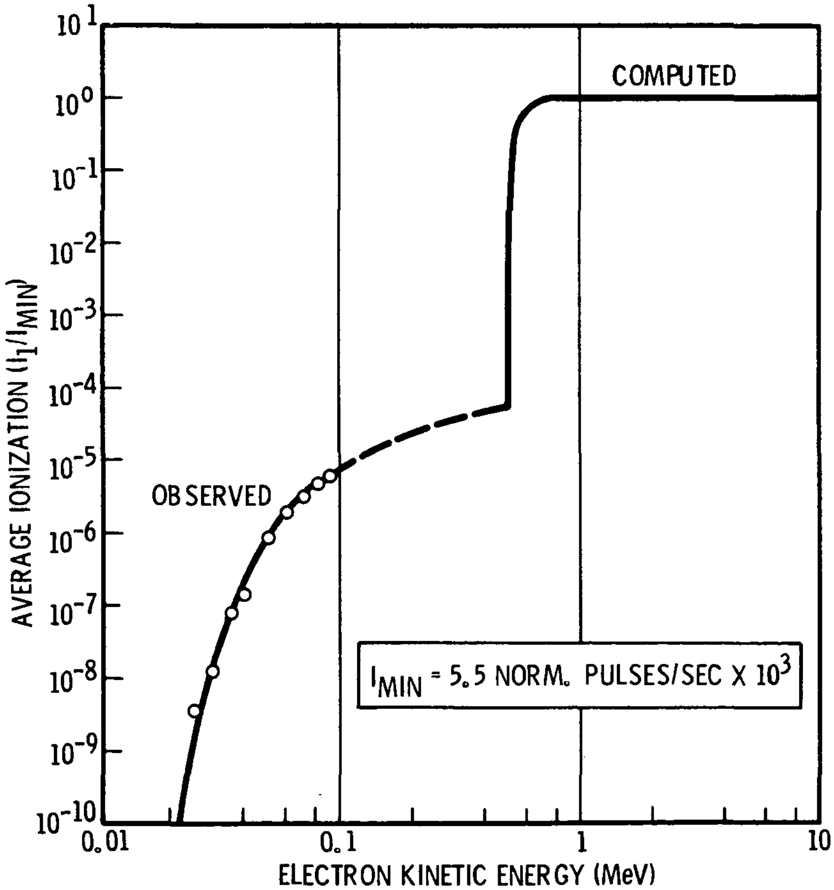

Figure 13. Ion Chamber Response Characteristics

counting all electrons with energy ≥ 0.7 MeV. That this is indeed true is indicated by comparison of electron fluxes measured with the electron spectrometer and those estimated from the ion chamber rates as in Figure 14 (Kane, 1967).

C. Presentation of the Data

Figures 15 and 16 show the ion chamber rates observed during two typical orbital passes of the OGO-3 satellite when the orbit was nearly equatorial (Figure 15) and when the orbit was inclined 50 degrees to the ecliptic (Figure 16). It can be seen that beyond the intensity maximum the pulsing rate of the chamber decreases more or less continuously with increasing radial distance, r, from the earth until the rate reaches the cosmic ray value in free space. The smallest value of the geocentric distance r at which the pulsing rate of the chamber becomes equal to the cosmic ray value is in most cases fairly well defined although rather large spikes superimposed on the cosmic ray rate may occasionally occur at larger geocentric distances. The boundary of the observable stable intensity of energetic electrons is defined here as the

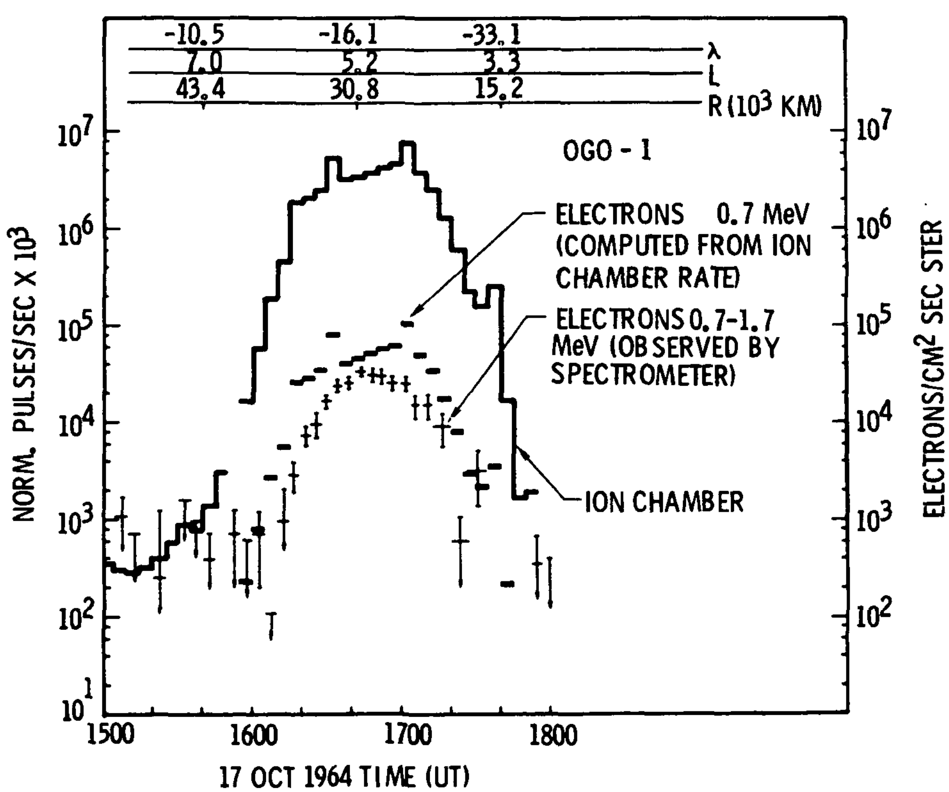

Figure 14. Comparison of Ion Chamber and Spectrometer

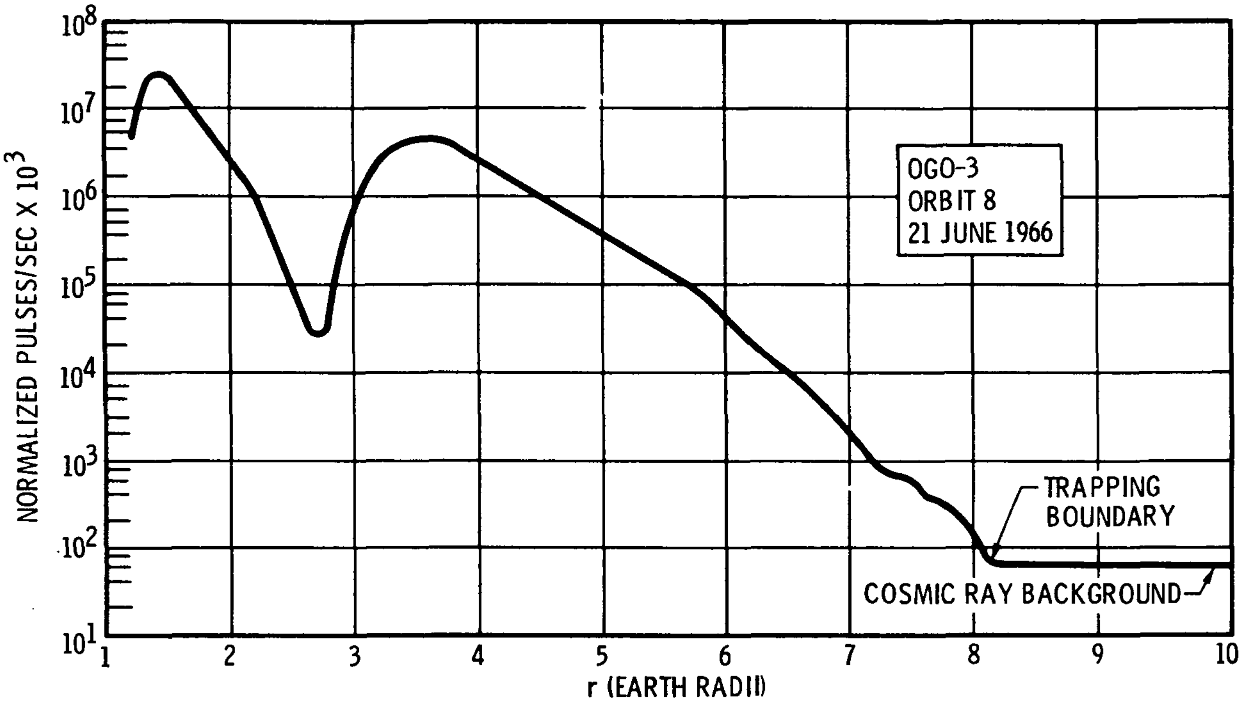

Figure 15. Sample Low Latitude Pass of OGO-3

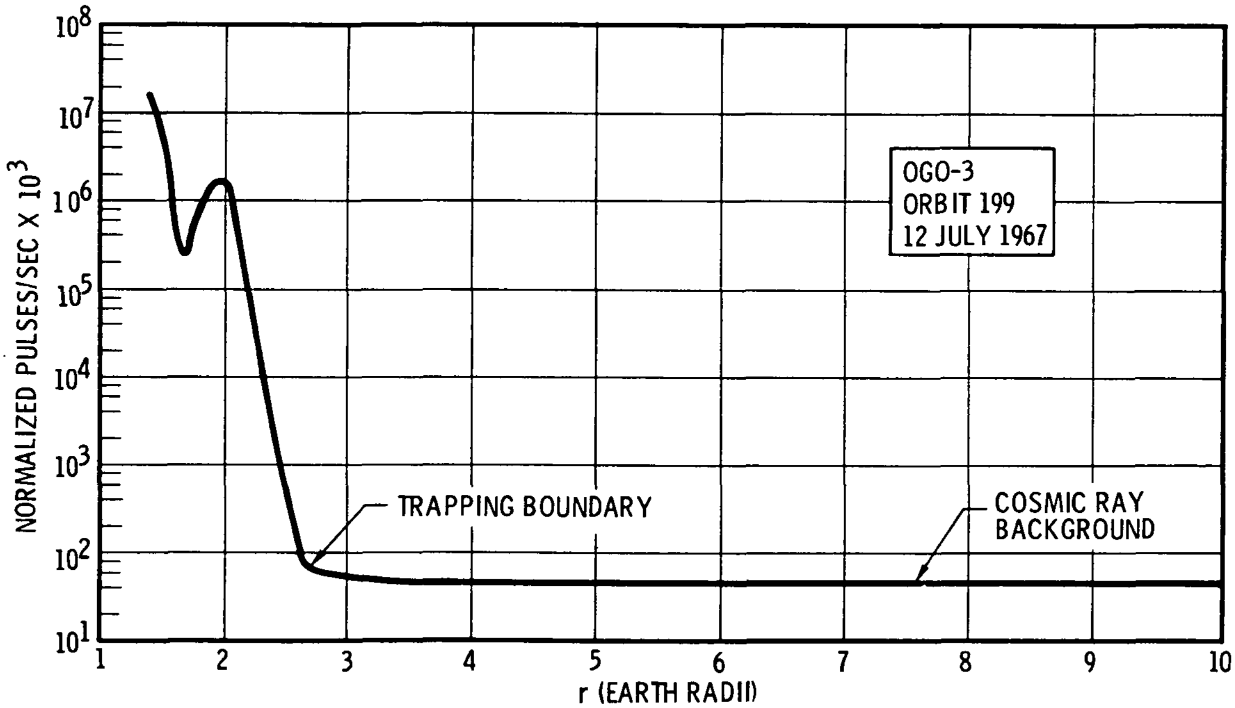

Figure 16. Sample High Latitude Pass of OGO-3

smallest radial distance at which the pulsing rate of the chamber becomes equal to that due to cosmic rays in free space.

The boundary defined here therefore applies to electron fluxes which can produce about 10 percent or more of the pulsing rate of the chamber due to cosmic rays. From Table I and Figure 13, it can be seen that the flux required to produce 10 percent of the cosmic ray rate is about 1 electron/cm^2 sec for electrons with energy ≥ 0.7 MeV and about 10^7 electrons/cm^2 sec for 40 keV electrons. Therefore the boundary as defined here applies primarily to electrons with energy ≥ 0.7 MeV. The boundary is the surface beyond which the flux of these energetic (≥ 0.7 MeV) electrons is less than 1 electron/cm^2 sec.

The objective of this investigation is to determine the location of this boundary as a function of latitude and local time under geomagnetically quiet conditions as well as to indicate any possible correlation with geomagnetic activity. For geomagnetically quiet conditions it was required than on the day of the measurement and the preceding day that $A_p \leq 15$. Also the data for the days immediately following a sudden commencement are rejected in order to avoid any short term fluctuations.

D. Latitude and Local Time Dependence

Before any quantitative estimates of the location of the boundary can be made it is essential to separate the latitude and local time dependence. To achieve this separation, separate studies of the latitude dependence are made in the following 4 magnetospheric sectors; noon (10-14 hrs LT), dusk (16-20 hrs), midnight (22-02 hrs) and dawn (04-08 hrs) (see Figures 17 through 21). We have determined that decreasing the local time intervals did not significantly reduce the scatter of data points, but increased the uncertainty in some of the intervals because of a lack of data samples. Although the quiet time data points (AP ≤ 15) are indicated differently from disturbed time data points (see Figures 18, 19, and 21), the removal of the disturbed time points does not significantly reduce the scatter of points or modify the best fit curve through the data points. Figures 20 and 21, which show the disturbed and

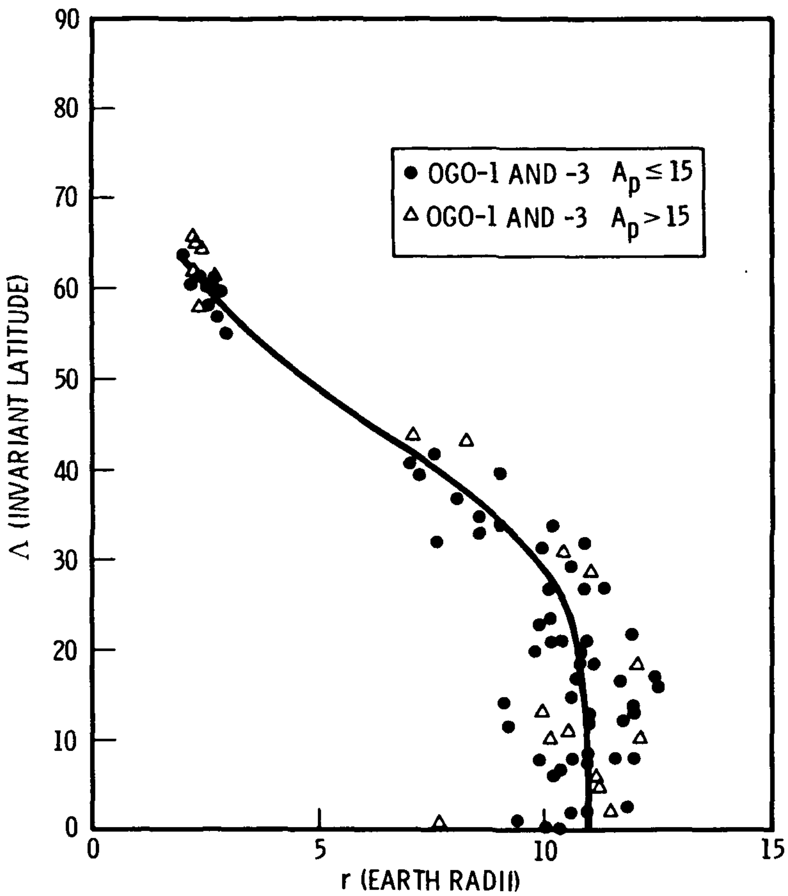

Figure 17. Latitude Dependence of Trapping Boundary at Noon (10-14 hrs LT)

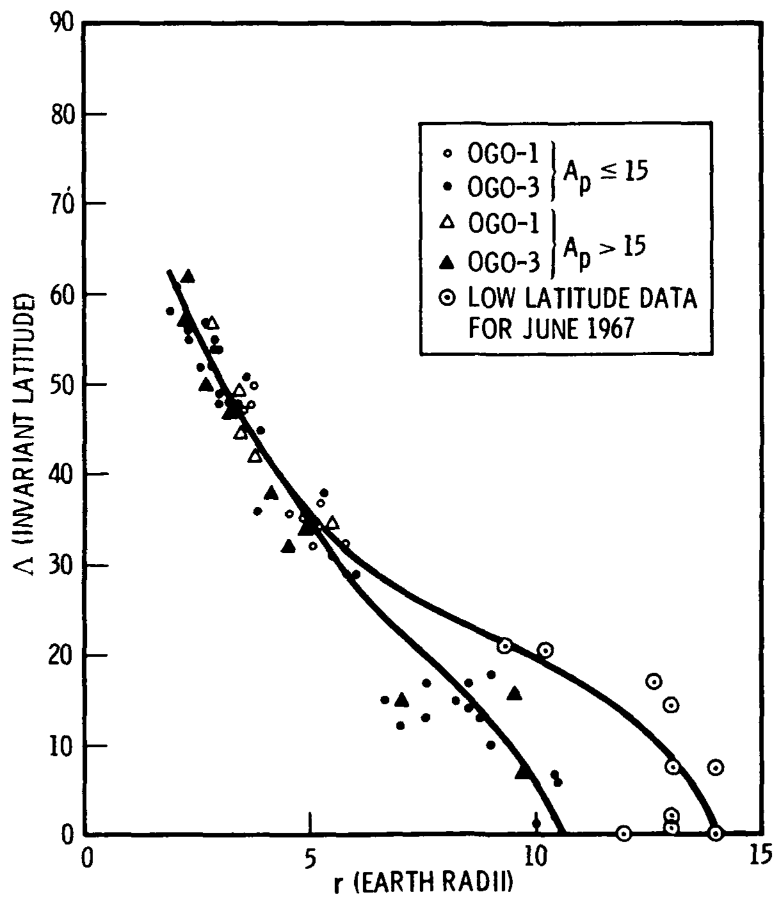

Figure 18. Latitude Dependence of Trapping Boundary at Midnight (22-02 hrs LT)

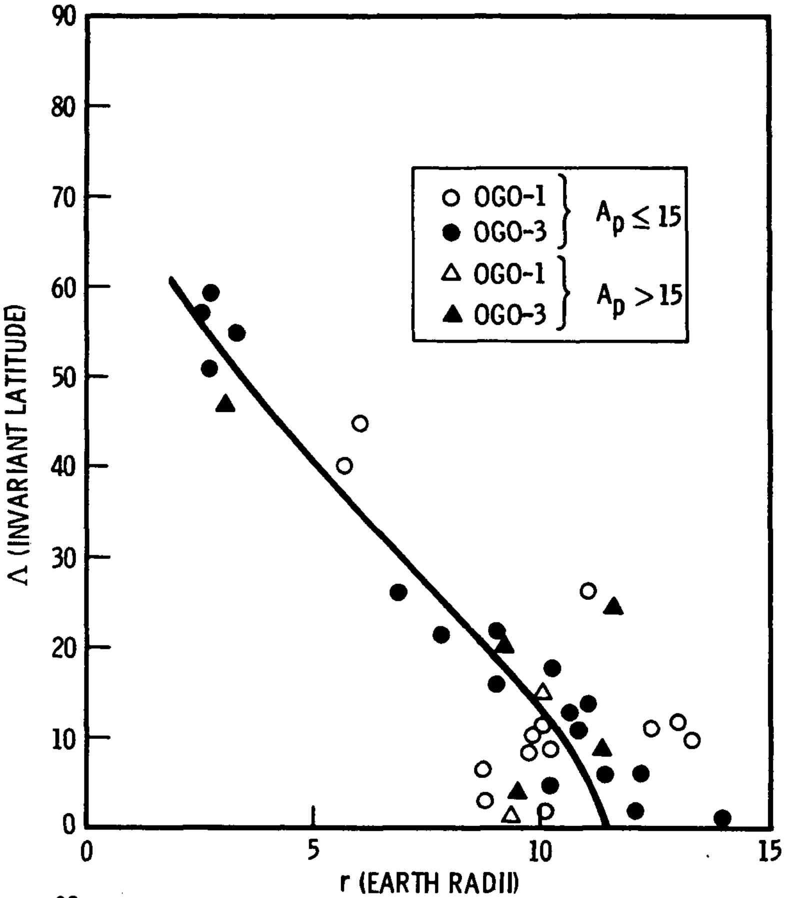

Figure 19. Latitude Dependence of Trapping Boundary at Dawn (04-08 hrs LT)

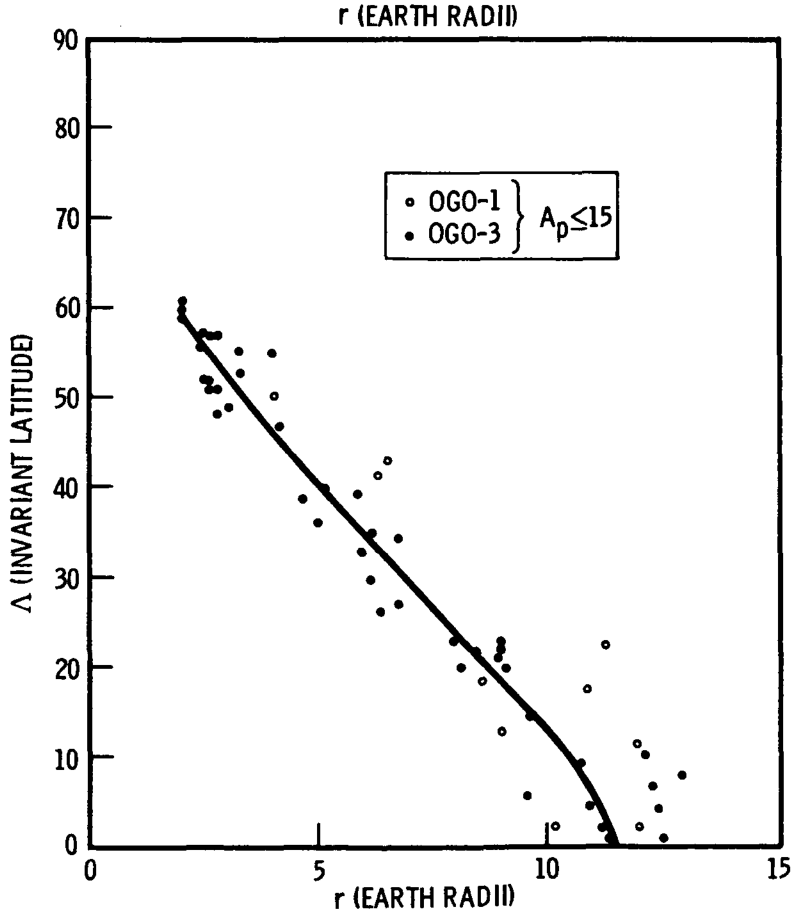

Figure 20. Quiet Time Latitude Dependence of the Trapping Boundary at Dusk (16-20 hrs LT)

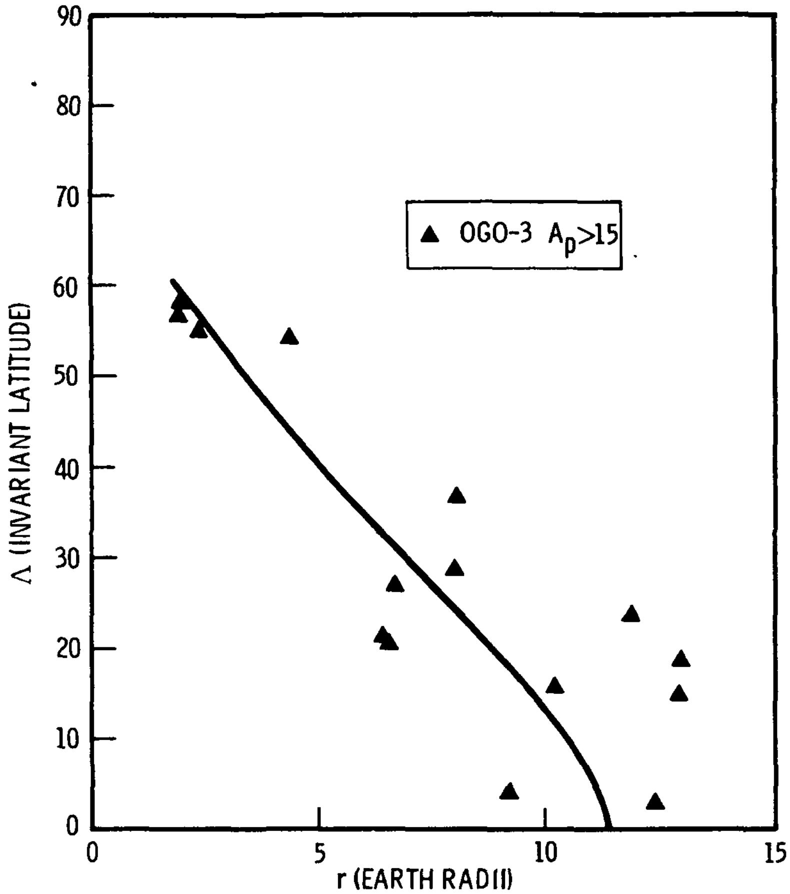

Figure 21. Disturbed Time Latitude Dependence of the Trapping Boundary at Dusk (16-20 hrs LT)

quiet time data points on separate plots, indicate that the best fit quiet time curve also represents the disturbed data accurately. We must conclude that magnetic activity is a poor indicator of the location of the stable trapping boundary for high energy electrons. The largest number of available data samples occurs for the noon (10-14 hrs LT) boundary determination. There is considerable variability in the location of the boundary; however, one can easily see that for $\Lambda < 30$ degrees the location of the boundary is sperical in nature (independent of Λ) as per theory (Mead, 1964).

The midnight points cluster along a well defined curve at higher latitudes but slow a large scatter at lower latitudes (see Figure 18). An investigation of this scatter indicates that the set of data points falling along the smaller r values were obtained in 1966, whereas those at the larger r range were obtained in 1967. The 1967 points were circled to point out this apparent time dependence. Since an apparent time dependence (which may be caused by some special magnetospheric conditions such as a long term difference in tail field strength) was observed in the midnight local time sector, the remainder of the data were analyzed for long-term-dependence. Each curve at a given longitude and latitude interval is made up of 3 or 4 sets of data separated in time by one year. One set is obtained per year as the satellite orbits move about one degree in local time per day. No further long-term time-dependence from the separate data sets was discernible in the remainder of the data within the observed day to day scatter.

The morning and evening sectors also show more scatter than the noon and midnight sectors, especially at low latitudes. However, this scatter can be attributed to the fact that in these sectors the ion chamber cut-off was not accurately measurable because the electron flux approached the cosmic ray background at an asymptotic rate, whereas in the noon midnight sector the cut-off is most often rapid and well defined. In preparation for a comparison of the data with the magnetic field models, a best fit curve has been drawn through the quiet time data points of Figures 17 through 20.

The equatorial crossing of the trapping boundary may be obtained by observing that within 15 degrees of the equator the trapping boundary is nearly spherical at all local times. Therefore, all of the boundary measurements with $\Lambda \leq 15$ degrees are plotted in Figure 22. The trapping boundary is approximately circular with a radius of 11 R_e. Furthermore, near local midnight all of the 1966 points fall outside of the 11 R_e circle; whereas, the 1967 points fall well inside the circle.

The high latitude earth intercept of the trapping boundary was determined by first determining the location of the boundary at 2.0 R_e. Figure 23 plots all of the data for $1.9\ R_e < r < 2.2\ R_e$ versus local time. We find that a circle intersecting local noon at 62 degrees and local midnight 58 degrees gives a best fit to the data. Since the trapping boundary follows the earths field lines at altitudes below 3 R_e, the above results are mapped to the earth's surface. A high latitude boundary is obtained at the earth's surface at 72 degrees at local noon, 70 degrees at dawn and dusk and 68 degrees at midnight. This result is in agreement with a number of other measurements (Vampola, 1971; McDiarmid, 1968; etc).

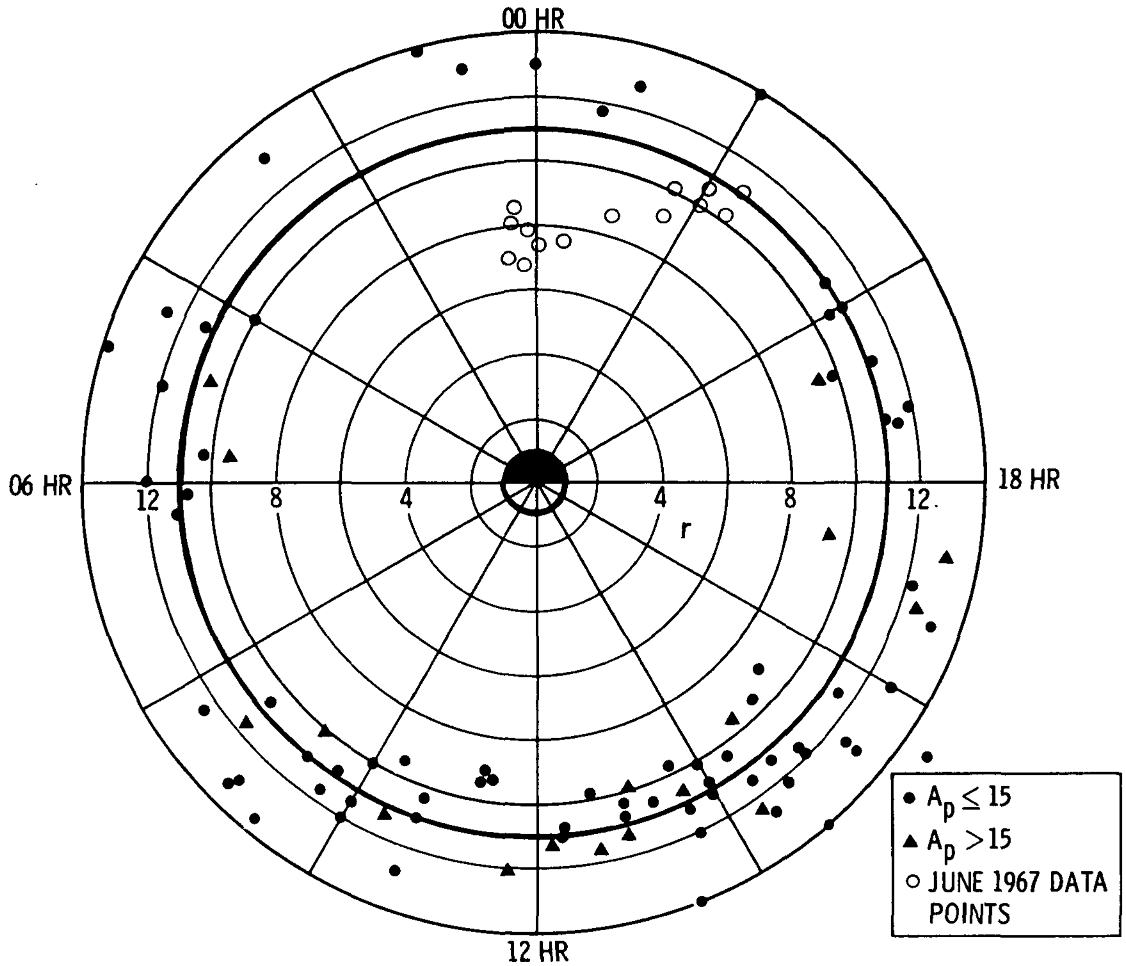

Figure 22. Equatorial Local Time Dependence of Trapping Boundary

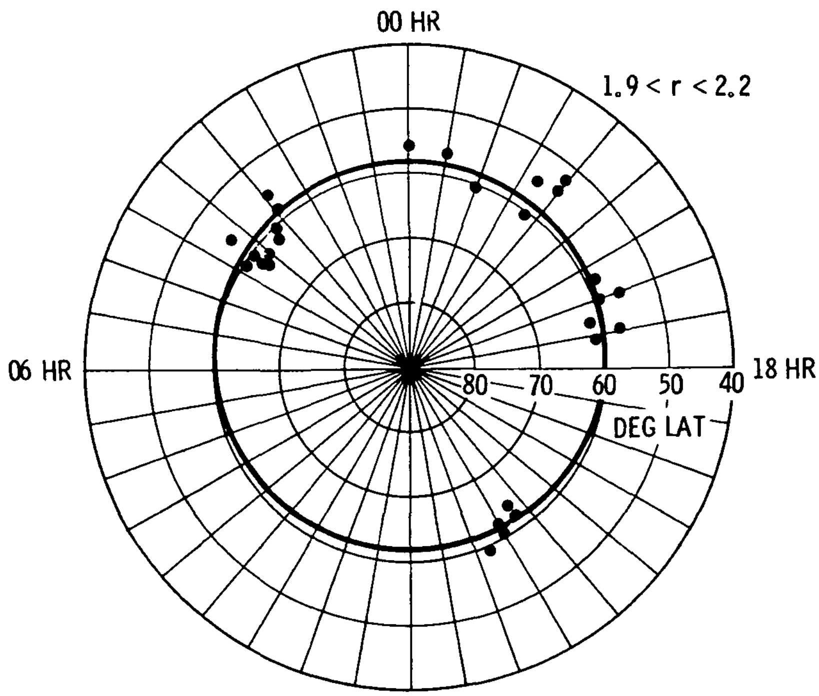

Figure 23. High Latitude Local Time Dependence of Trapping Boundary

E. Discussion of the Models

The above data may be compared to the predictions of field line and drift shell geometries predicted by several models. The data were compared to the Mead-Williams model (Williams and Mead, 1965), to the Olson tilted model (Olson, 1970) and Mead-Fairfield empirical model (Mead and Fairfield, 1971). Since the region of interest included the region at the front edge of the tail where the Mead-Williams model contains a singularity the Mead-Williams model could only be used for field line geometries near local noon. Near local noon the Mead-Williams model gave results which were similar to the results of the Olson 0 degree tilt model and hence the Mead-Williams model will not be further discussed in this study.

The models were used to generate the last closed drift shell on which high energy electrons can be permanently trapped (i.e., drift completely around the earth). Because of the distortion in the field one cannot simply calculate the drift shell for a given particle but must consider particles of various pitch angles. It has already been shown that drift shell splitting in the distorted magnetosphere is important at 6.6 R_e (Pfitzer et al., 1969). At larger distances the distortion is even greater and hence the shell splitting becomes more important. The basic analysis programs used were the electric field free (electric fields are not important for 700 keV electrons) drift shell program of J. Roederer which uses McIlwain's field line tracing program. Electrons with differing pitch angles and differing equatorial starting points were allowed to computer drift around the earth using the Olson (tilt = 0 degrees), and the Mead-Fairfield magnetic field models.

As the particles were started closer and closer to the boundary (which was set at 10.5 R_e and 11.0 R_e for Olson's model) difficulties were encountered in both models. The Mead-Fairfield model began to predict two magnetic field minima near a latitude of about ±40 degrees and distances greater than >10 R_e. Although this prediction is in accordance with observations the existing drift shell program assumes the equator to be defined as the minimum magnetic field position and, therefore, does not predict the correct drift shells in these cases. The program must be modified in order to generate believable results in the case of double magnetic field minima. In

Olson's model there is a tendency for the field expansion to begin diverging as the boundary is approached and no useful drift shells can be computed for radial distances greater than 10 R_e. We find that this is caused by the fact that spherical harmonic expansions are used which are valid inside a 10.5 R_e sphere (when the standoff distance is 10.5 R_e) but near the edge of the sphere the series rapidly begins to diverge as might be expected. We therefore are limited to discuss field lines having equatorial crossing distance near noon no greater than 10 R_e.

Since the ion chamber is an omnidirectional instrument it gives no pitch angle information and a given particle which follows a specific drift shell cannot be observed. Instead we observe a collection of all pitch angles and the observed trapping boundary is constructed of particles having varying pitch angles. Olson's model, for example, predicts that particles having equatorial pitch angles > 80 degrees when inserted at noon at 10 R_e drift on closed drift shells; however, particles having equatorial pitch angles < 80 degrees when inserted at noon at 10 R_e drift out into the tail. Calculations of particle trajectories indicate that $r = 9.5$ R_e is the largest distance at noon at which particles of all pitch angles can exist on closed drift shells. Figure 24 shows drift shells for particles crossing local noon at 9.5 R_e. Particles having a pitch angle of 90 degrees cross the midnight longitude at a distance of 7.6 R_e and particles having a pitch angle of 7 degrees cross the midnight longitude at 11.5 R_e.

Similarly it is found that particles having an equatorial crossing at 10 R_e near local midnight also exhibit the same type of drift shell splitting. Particles with small pitch angles can successfully drift around the earth whereas particles with a pitch angle of 90 degrees drift out of the sides of the magnetosphere.

It can be concluded that near midnight the trapping boundary is made up of particles having small equatorial pitch angles and hence the trapping boundary closely approximates the shape of a field line near midnight. At noon, however, the trapping boundary is not determined by particles trapped on a single field line but is a combination of particles mirroring at different

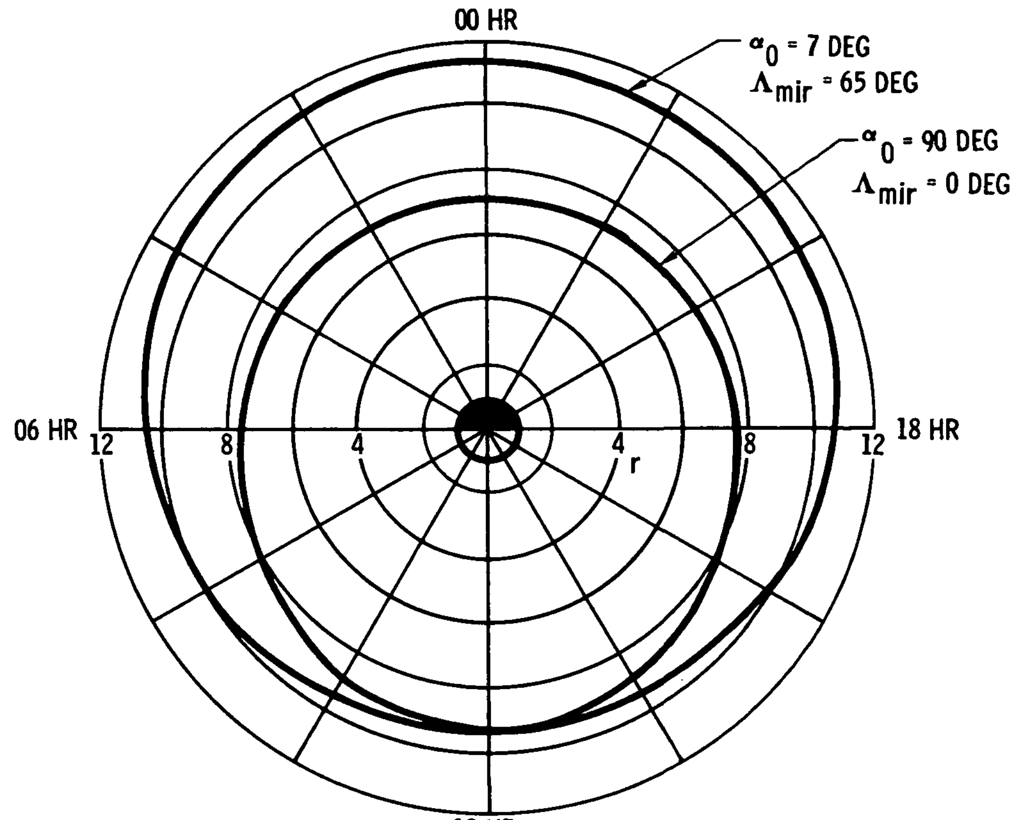

Figure 24. Equatorial Drift Shell Intercepts as Calculated from Olson's Model

latitudes and equatorial crossings. At high latitudes the trapping boundary consists of particles having small equatorial pitch angles and crossing the equator at 9.5 R_e. However, near the equator particles having pitch angles of 80 degrees can exist on closed drift shells out to distances $> 10\ R_e$. Figure 25 demonstrates the predicted boundary at noon and midnight. At noon we note that the trapping boundary (solid curve) is a composite of several field lines (dashed curve) whereas at midnight the trapping boundary is coincident with a single field line. There exists a region extending from the earth to 9.5 R_e at noon and to 7.5 R_e at midnight where particles of all pitch angles may be trapped. Outside of this region there is a region at noon where only particles with large equatorial pitch angles are trapped and there is a region at midnight where only particles with small equatorial pitch angles are trapped.

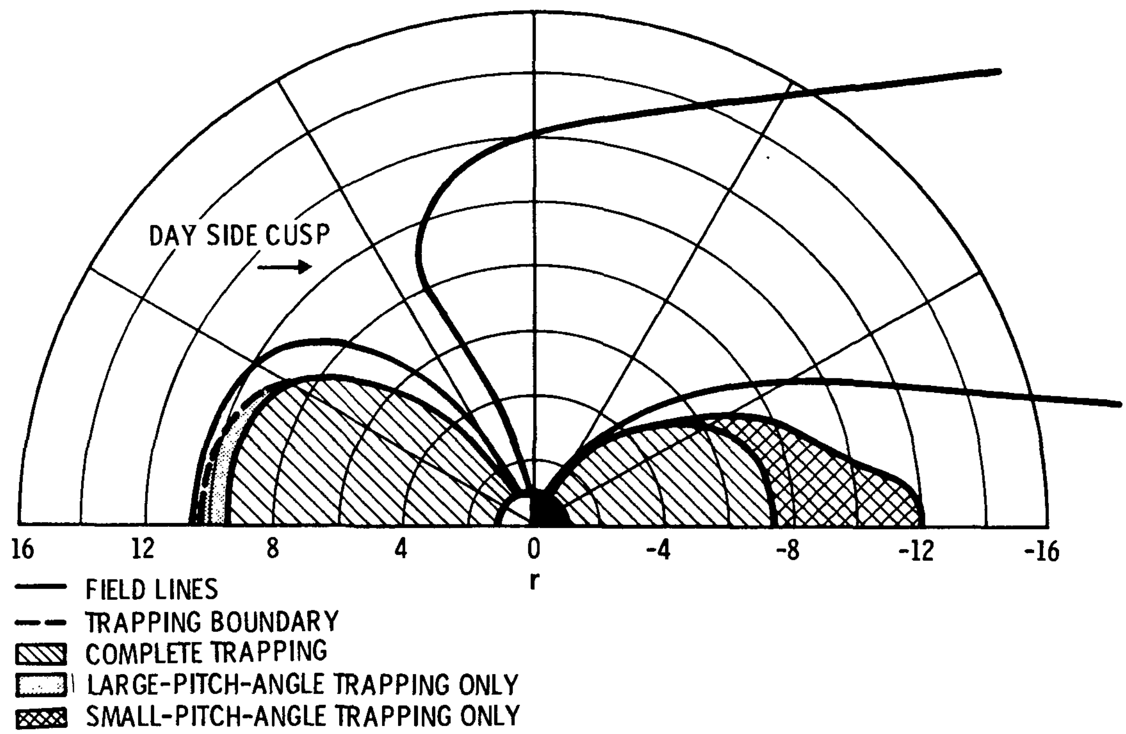

Figure 25. Noon and Midnight Meridian Cross-section of Trapping Regions

F. Comparison of Data and Models

The best fit experimentally determined trapping boundary compared with the calculated curves using Olson's and Mead-Fairfield's models are shown in Figures 26 and 27. We note that both at noon and midnight the empirical model of Mead-Fairfield (a model which is a least square polynomial fit to all available magnetometer measurements) more closely approximates the data that does Olson's model (a model which is derived from first principles involving pressure balance and current flows on the magnetospheric boundary and tail). The agreement with Mead-Fairfield's model is probably within the experimental error of this determination of the boundary and the determination of the magnetic field by Mead-Fairfield from available magnetometer data. The differences between Olson's model and the data is caused by the fact that Olson's model (as well as all other mathematical models) do not yet include the distributed currents flowing within the magnetosphere. Olson has indicated (private communications) that several of these studies have indicated the importance of distributed currents within the magnetosphere, and that

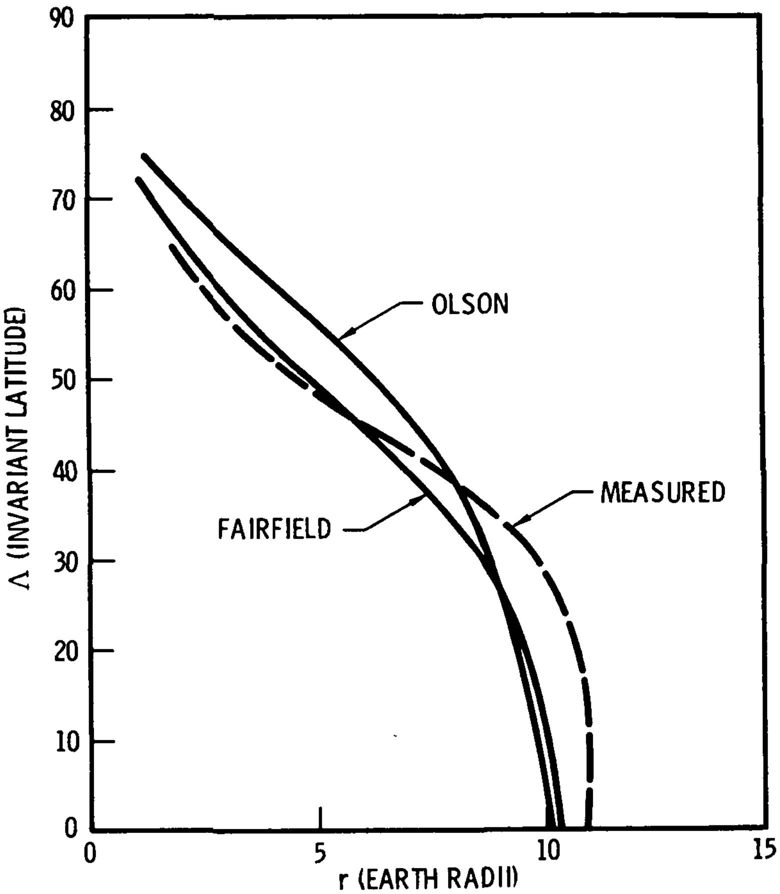

Figure 26. Comparison of Observed and Calculated Trapping Boundary at Noon

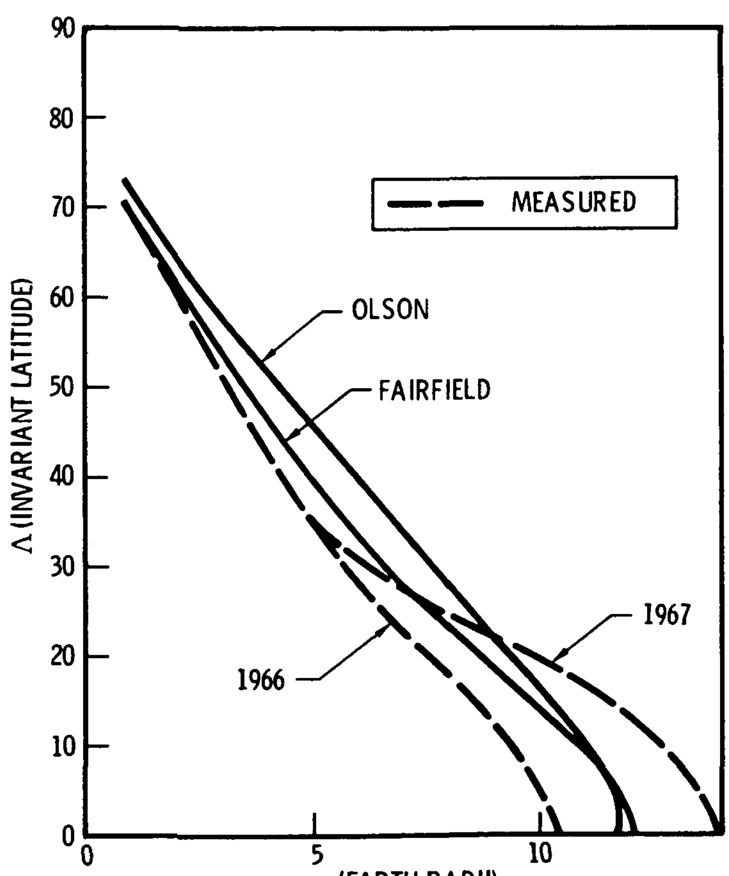

Figure 27. Comparison of Observed and Calculated Trapping Boundary at Midnight

these currents will be included in a later version of the model. The discrepancies between model and data are largest at approximately 5 R_e. It is not possible to juggle tail field strengths or stand-off distance to bring the model into agreement with the data. At $\Lambda = 0$ degrees the model with appropriate choices of R_S, the stand-off distance, and tail field strength can easily be made to fit the data. Olson's model correctly predicts, for example, both the diurnal as well as seasonal changes of the magnetic field at synchronous orbit. One therefore concludes that in order for the model to fit the observed trapping boundary, currents other than tail currents and magnetopause currents must play an important role near 5 R_e and latitudes of ~ 40 degrees. A study of the long term time dependence observed at midnight showed that by increasing or decreasing the tail field strength, the calculated curve plotted inFigure 27 can be made to more closely agree with either one of the two experimental branches. Thus indicating that changes in the strength of the tail field can account for the difference between the two observed curves.

As discussed in Section D the high latitude intercept of the trapping boundary with the earth is at 72 degrees at noon and at 68 degrees near midnight. Table II has been formulated to bring together a number of measurements which are directly or indirectly related to the high latitude earth intercept of the trapping boundary. All of the experimental data values, the determination of the location of the trapping boundary, the location of the Dayside Cusp, the location of the Plasma Cusp, the first open field line, and the cosmic ray cut-off form a consistent set. The trapping boundary is located at 72 degrees at noon, the cosmic ray cut-off is 4 degrees lower in latitude and the dayside cusp is about 4 degrees higher in latitude and the 1st open field line is in the region of the dayside cusp. When this data is compared with predictions of the magnetic field models we find that Olson's model predicts latitudes which are consistently 4-6 degrees higher and Mead-Fairfield's model predict latitudes which are consistently 2-4 degrees higher.

Table II

EXPERIMENTAL

	OGO-1 & 3 Trapping Boundary	Dayside Cusp(1)	Plasma Cusp	1st Open Field Line (OGO-6)(2)	OGO-6 Cut-off (5 MeV)(3)
Noon	72° ± 2°	75° - 79°	-	76°	68°
Midnight	68° ± 2°	-	68°	-	63°

(1) Heikkila and Winningham, 1971.

(2) Masley et al., 1971b..

(3) Masley et al., 1971a.

THEORETICAL

	Trapping Boundary Closed Magnetosphere		1st Open Field Line		Cut-off	
	Olson	Mead-Fairfield	Olson	Mead-Fairfield	Olson	Mead-Fairfield
Noon	76°	73°	81°	78°	74°	72°
Midnight	72°	70°	-	-	69°	68°

The above result may have a direct bearing on the discrepancey between calculated and measured cosmic ray trajectories. It is well known that the models (in particular the Mead-Williams and Olson models) predict cosmic ray cut-offs which are much too high (Masley et al., 1971a). The identical models which were used to calculate the cosmic ray cut-offs were also used in this boundary study. It is found that the discrepancy between the calculated and observed trapping boundary is of the same order as the discrepancy between calculated and observed cosmic ray cut-offs. An adjustment to the models to give better agreement between the calculated and measured trapping boundary location would also lower the cosmic ray cut-offs and bring the calculated cut-offs into better agreement with the experimentally measured cut-offs.

V. SUMMARY

This study has determined the radial diffusion coefficient in the inner zone for $1.6 \leq L \leq 2.2$ for electrons having a first invariant of $\mu = 12$ MeV/gauss. The coefficient determined by this study, which is larger than some of the earlier values obtained by (Newkirk and Walt, 1968), gives rise to the possibility that there exists a lower limit to the fluxes in the inner zone because of a continuous diffusive resupply through the slot between the inner and outer zone. It is expected, however, that the major source of electrons for the inner zone will continue to be the single injections of major magnetic storms.

We have also demonstrated that by using the solar wind pressure as an input to the magnetic field models the agreement between observed and calculated magnetic fields as well as between observed and calculated particle fluxes is improved. In particular, changes in the plasma pressure can cause apparent local time asymmetries in the particle flux. It has been shown that the apparent asymmetry on February 15, 1967 is instead a time dependent solar wind induced fluctuation. It has been demonstrated that by including solar wind pressure information into the magnetic field models, significant improvement is obtained in correlating experimental and theoretical results. Future work, in particular, studies of magnetic fields and particle fluxes in the outer zone which utilize magnetic field models, should input available plasma pressure data into the model calculations.

A further comparison of the magnetic field models with the observed location of the trapping boundary indicates the need for the inclusion of distributed currents within the magnetosphere. Olson's independent studies (private communication) have also indicated a need for the inclusion of these currents in the models in order that his magnetic field values more closely agree with measured values. The above study can then be used as an independent check on the new magnetospheric field configuration.

It has also been shown that the high latitude trapping boundary is only weakly A_p dependent and that the plasma pressure when used to calculate the stand-off distance improves the accuracy of the models. Therefore, the trapping boundary study can be significantly improved (i. e. the scatter of points reduced significantly) by incorporating a stand-off distance which varies with the plasma pressure. (These data are available from the National Data Center.) By improving the boundary shape determination it may be possible to directly predict the location of the distributed currents with the magnetopause.

REFERENCES

Fairfield, D.H., Trapped particles in a distorted dipole field, J. Geophys. Res., 69, 3919, 1964.

Farley, T.A., Radial diffusion of electrons at low L values, J. Geophys. Res., 74, 377, 1969.

Frank, L.A., Inward radial diffusion of electrons greater than 1.0 million electron volts in the outer radiation zone, J. Geophys. Res., 70, 3533, 1965a.

Frank, L.A., Observations of magnetospheric boundary phenomena, presented at the advanced study institute "Radiation trapped in the earth's magnetic field" in Bergen, Norway, August 16-September 3, 1965b.

Heikkila, W.J., and J.D. Winningham, Penetration of magnetosheath plasma to low altitudes through the dayside magnetospheric cusps, J. Geophys. Res., 76, 883, 1971.

Hones, E.W., Jr., Motion of charged particles trapped in the earth's magnetosphere, J. Geophys. Res., 68, 1209, 1963.

Kane, S.R., Application of an integrating type ionization chamber to measurements of radiation in space, Ph.D. Thesis, University of Minnesota Cosmic Ray Technical Report CR-106, September, 1967.

Lezniak, T.W., R.L. Arnoldy, G.K. Parks, and J.R. Winckler, Measurement and intensity of energetic electrons at the equator at 6.6 R_e, Radio Science, 3, 710, 1968.

Lezniak, T.W. and J.R. Winckler, The structure of the magnetopause at 6.6 R_e in terms of 50-150 keV electrons, J. Geophys. Res., 73, 5733, 1968.

Masley, A.J., W.P. Olson, and K.A. Pfitzer, Calculations of charged particle entry into the polar regions, Conf. Papers, 12th Intl. Conf. on Cosmic Ray, Hobart, Australia, 2, 824, 1971a.

Masley, A.J. and P.R. Satterblom, Solar cosmic ray observations during the September and November 1969 events, Conf. Papers, 12th Intl. Conf. on Cosmic Rays, Hobart, Australia, 5, 1849, 1971b.

McDiarmid, I.B., and J.R. Burrows, Local time asymmetries in the high latitude boundary of the outer radiation zone for the different electron energies, Can. J. Phys., 46, 49, 1968.

Mead, G. D., Deformation of the geomagnetic field by the solar wind, J. Geophys, Res., 69, 1181, 1964.

Mead, G. D., The motion of trapped particles in a distorted magnetosphere, in Radiation Trapped in the Earth's Magnetic Field, Proc. Advan. Study Inst., Bergen, Norway, August 1965, edited by B. M. McCormac. pp. 481-490, D. Reidel Publishing Company, Dordrecht-Holland, 1966.

Mead, G. D., and D. H. Fairfield, Quantitative magnetospheric models derived from satellite magnetometer data, presented to the XVth General Assembly of IUGG, Moscow, 1971.

Newkirk, L. L., and M. Walt, Radial diffusion coefficient for electrons at $1.7 < L < 5$, J. Geophys. Res., 73, 7231, 1968.

Northrop, T. G., and E. Teller, Stability of the adiabatic motion of charged particles in the earth's field, Phys. Rev., 117, 215, 1960.

Olson, W. P., A scalar potential representation of the tilted magnetopause and neutral sheet magnetic fields, presented at the Boulder Conference on Quantitative Magnetospheric Models, McDonnel Douglas Astronautics Company Paper WD-1332, 1970.

Pfitzer, K. A., An experimental study of electron fluxes from 50 keV to 4 MeV in the inner radiation belt, Ph. D. Thesis, University of Minnesota Cosmic Ray Technical Report CR-123, August, 1968.

Pfitzer, K. A. and J. R. Winckler, Experimental observation of a large addition to the electron inner radiation belt after a solar flare event, J. Geophys. Res., 73, 5792, 1968.

Pfitzer, K. A., and J. R. Winckler, Intensity correlations and substorm electron drift effects in the outer radiation belt measured with the OGO-III and ATS-1 satellites, J. Geophys, Res., 74, 5005, 1969, and University of Minnesota Cosmic Ray Technical Report CR-136, April, 1969.

Pfitzer, K. A., T. W. Lezniak, and J. R. Winckler, Experimental verification of drift shell splitting in the distorted magnetosphere, J. Geophys, Res., 74, 4687, 1969.

Roederer, J. G., On the adiabatic motion of energetic particles in a model magnetosphere, J. Geophys,, 72, 981, 1967.

Roederer, J. G., Quantitative models of the magnetosphere, Rev. Geophys., 7, 1969.

Vampola, A. L., Access of solar electrons to closed field lines, J. Geophys. Res., 76, 36, 1971.

Walt, M., Radial diffusion of trapped particles and some of its consequences, Rev. Geophys., 9, 11, 1971.

Williams, D. J. and G. D. Mead, Nightside magnetosphere configuration as obtained from trapped electrons at 1100 kilometers, J. Geophys. Res., 70, 3017, 1965.